The Response of the Large-Scale Tropical Circulation to Warming

Levi G. Silvers[1], Kevin A. Reed[1], Allison A. Wing[2]

[1]School of Marine and Atmospheric Sciences, State University of New York at Stony Brook, Stony Brook, NY, USA
[2]Department of Earth, Ocean, and Atmospheric Science, Florida State University, Tallahassee, FL, USA

Key Points:

- The overturning tropical circulation weakens as the surface warms in the majority of RCE models examined.
- The inter-model spread of the change with warming can be explained by the mean upward velocity at 500 hPa.
- Variability of the clear-sky heating and static stability result in large variations of the subsidence velocity.

Corresponding author: Levi G. Silvers, `levi.silvers@stonybrook.edu`

Abstract

Previous work has found that as the surface warms the large-scale tropical circulations weaken, convective anvil cloud fraction decreases, and atmospheric static stability increases. Circulation changes inevitably lead to changes in the humidity and cloud fields which influence the surface energetics. The exchange of mass between the boundary layer and the midtroposphere has also been shown to weaken in global climate models. What has remained less clear is how robust these changes in the circulation are to different representations of convection, clouds, and microphysics in numerical models. We use simulations from the Radiative-Convective Equilibrium Model Intercomparison Project (RCEMIP) to investigate the interaction between overturning circulations, surface temperature, and atmospheric moisture. We analyze the underlying mechanisms of these relationships using a 21-member model ensemble that includes both general circulation models and cloud resolving models. We find a large spread in the change of intensity of the overturning circulation. Both the range of the circulation intensity, and its change with warming can be explained by the range of the mean upward vertical velocity. There is also a consistent decrease in the exchange of mass between the boundary layer and the midtroposphere. However, the magnitude of the decrease varies substantially due to the range of responses in both mean precipitation and mean precipitable water. This work implies that despite well understood thermodynamic constraints, there is still a considerable ability for the cloud fields and the precipitation efficiency to drive a substantial range of tropical convective responses to warming.

Plain Language Summary

Tropical large-scale overturning circulations are expected to weaken with warming. This weakening is the result of precipitation increasing at a slower rate than does atmospheric water vapor. Because precipitation and water vapor are important measures of how energy flows through the atmosphere it is important to understand how they will respond to a warming climate. We use two methods to calculate the change of the overturning circulation in 21 different numerical models that simulate the tropical atmosphere. This group of models includes high resolution models that resolve cloud systems, and global models with grid-spacing of about 100 km. We show that a weakening circulation that results from increasing stability, atmospheric cooling, and latent heat flux from the surface is a robust result across most models. But across the group of models there is a large range of magnitudes in the response of the circulation to warming. This variability is well explained by the magnitude of the mean upward vertical velocity. High resolution models do not narrow the range of responses. Narrowing this range of responses will depend on developing a better understanding of what drives the variations in stability, surface fluxes of latent energy, and relative humidity.

1 Introduction

Progress has been made in recent work that has contributed to a better understanding of how Earth's climate will respond to increasing concentrations of greenhouse gases (GHG). The expected global mean thermodynamic and hydrologic response to GHG forcing is becoming clearer and the range of anticipated feedback responses to GHG forcing is narrowing (Sherwood et al., 2020). However, predicting and understanding how dynamic circulations, local feedback processes, and regional precipitation characteristics will adjust to changes in the climate remains challenging (Shepherd, 2014; Voigt & Shaw, 2015). The circulation of the atmosphere is a critical determining factor in the location of regional changes to weather and climate, with direct consequences for society. While changes of circulation are predicted to result from the warming of Earth's climate, there is a large range in the circulation patterns and characteristics projected by the current generation of comprehensive global climate models.

There is evidence that the Earth's large-scale overturning circulation, often characterized by the Hadley and Walker Circulations, will decrease in strength as the global mean temperature increases. A decrease with warming of the convective mass flux of the atmosphere has been shown to be a straightforward result of atmospheric thermodynamic constraints (Betts & Ridgway, 1988; Held & Soden, 2006). This weakening tropical overturning circulation is a robust feature of many global climate models (Knutson & Manabe, 1995; Held & Soden, 2006; Vecchi & Soden, 2007; Bony et al., 2013; Medeiros et al., 2015). Physical understanding of this decrease can be traced back to Betts and Ridgway (1988) who showed that because a typical rate of increase of precipitation (often $\sim$ 2%/K) is weaker than the increase of water vapor that is constrained by the Clausius-Clapeyron (CC) relation ($\sim$ 7%/K), a slowdown of the mass exchange between the atmospheric boundary layer (BL) and the overlying troposphere can be expected. Increasing surface temperatures can also lead to an increase of the atmospheric static stability (Bony et al., 2016). The deep, convective activity in the tropics acts to drive the ambient temperature towards the moist adiabat. Gravity waves then act to quickly drive most of the tropical troposphere towards the temperature that is largely set by the deep convection. Both the deep convection and the overturning circulation influence the amount of water vapor in the free-troposphere which, in combination with the tropospheric temperature, acts to determine the atmospheric radiative cooling that constrains the domain mean precipitation. This picture of warming-induced changes that include a weakening tropical circulation and subsidence velocity along with an increasing static stability and residence time of water vapor has become fairly clear in the literature of recent decades (Jenney et al., 2020).

However, some important questions remain. For example, how robustly do models of RCE represent these warming induced changes to the circulation? How does the circulation response to warming in RCE simulations compare between General Circulation Models (GCMs) and Cloud-system Resolving Models (CRMs) despite the large difference in grid-spacing of the two model types? Many previous studies have looked at overturning circulations in observations or in general circulation models (GCMs) in which the circulations are clearly linked to large-scale temperature gradients, spatial differences in the insolation, and the rotation of Earth (e.g., Held & Soden, 2006; Medeiros et al., 2015). The large-scale circulations of RCE simulations are driven not by large-scale temperature gradients at the surface or in the insolation, but by a combination of the radiatively driven subsidence and the convective activity.

The relation between Earth's observed tropical large-scale circulation and circulations that are generated in RCE simulations is not obvious *a priori*. A common metric of the large-scale circulation is the vertical pressure velocity on the 500 hPa pressure surface (ω_{500}). Remarkably, the probability distribution function of ω_{500} is similar among RCE simulations, Aquaplanet simulations, *amip* simulations, and reanalyses that are heavily dependent on observations (Bony et al., 2004; Medeiros et al., 2015; Cronin & Wing, 2017). The similarity is due not primarily to the regions of deep convection, but rather to subsiding regions of the tropics where the dominant statistical weight of moderately subsiding air ($\approx 10 - 20\,\mathrm{hPa/day}$) indicates the large number of shallow clouds in the BL. This can be seen as evidence that the distribution of the large-scale dynamic regimes in the tropics is driven by the clear sky radiative cooling rate. The observed similarity of dynamic regimes encourages further research into the physical mechanisms and coupling processes between clouds and the circulation that could be common between the observed atmosphere, Earth-like simulations, and various models of RCE.

This study focuses on the intensity, and the change of intensity with warming, of the large-scale circulation that is created entirely by the interactions between atmospheric radiation and convection across a large range of models that participated in the Radiative-Convective Equilibrium Model Intercomparison Project (RCEMIP; Wing et al., 2018). One of the goals of this work is to provide context for studies of the tropical overturn-

Table 1: List of Models that are used in this study and that participated in RCEMIP. The colors used to identify models are the same as those used in Wing et al. (2020).

Model abbreviation	Model name	Model type	Color
CAM5-GCM	Community Atmosphere Model v5	GCM	
CAM6-GCM	Community Atmosphere Model v6	GCM	
CNRM-CM6-1	Atmospheric component of the CNRM Climate Model 6.1	GCM	
ECHAM6-GCM	MPI-M Earth System Model-Atmosphere component v6.3.04p1	GCM	
GEOS-GCM	Goddard Earth Observing System model v5.21	GCM	
ICON-GCM	ICOsahedral Nonhydrostatic Earth System Model-Atmosphere component	GCM	
SAM0-UNICON	Seoul National University Atmosphere Model v0	GCM	
SP-CAM	Super-Parameterized Community Atmosphere Model	GCM	
SPX-CAM	Multi-instance Super-Parameterized CAM	GCM	
UKMO-GA7.1	UK Met Office Unified Model Global Atmosphere v7.1	GCM	
ICON-LEM	ICOsahedral Nonhydrostatic-2.3.00, LEM	CRM	
ICON-NWP	ICOsahedral Nonhydrostatic-2.3.00, NWP	CRM	
MESONH	Meso-NH v5.4.1	CRM	
SAM-CRM	System for Atmospheric Modeling 6.11.2	CRM	
SCALE	SCALE v5.2.5	CRM	
UCLA-CRM	UCLA Large-Eddy Simulation model	CRM	
UKMO-CASIM	UK Met Office Idealized Model v11.0 - CASIM	CRM	
UKMO-RA1-T	UK Met Office Idealized Model v11.0 - RA1-T	CRM	
UKMO-RA1-T-nocloud	UK Met Office Idealized Model v11.0 - RA1-T	CRM	
WRF-COL-CRM	Weather Research and Forecasting model v3.5.1	CRM	
WRF-CRM	Weather Research and Forecasting model v3.9.1	CRM	

ing circulation when forced either by idealized SST patterns that generate a mock-Walker circulation (e.g. Raymond, 1994; Grabowski et al., 2000; Tompkins, 2001; Bretherton & Sobel, 2002; Lutsko & Cronin, 2018; Silvers & Robinson, 2021) or by observed Earth-like conditions (Vecchi and Soden, 2007). Our analysis is driven largely by these two questions:

1. How does the overturning circulation change with warming in the RCEMIP multi-model ensemble?
2. What controls the intermodel spread in the circulation strength and the change with warming?

The remainder of this paper is organized as follows. The RCEMIP configurations, experiments used, and analysis methods are described in section 2. Section 3 calculates the change of circulation with warming. This is done with two different methods, and the connection between the methods is discussed. In section 4 we illustrate some of the sources of intermodel spread. This includes section 4.1 which discusses the role of the surface energy flux and precipitation on the overturning circulation and section 4.2 which illustrates the range of variability of the static stability and relative humidity. The main conclusions and final comments are presented in section 5.

2 Experiments and Methods

All experiments used in this paper follow the RCEMIP protocol and experiments documented by Wing et al. (2018, 2020). Throughout this paper we have used the same colors and model abbreviations to identify models as in Wing et al. (2020), see Table 1. A brief description of the experiments follows. Radiative Convective Equilibrium (RCE) is simulated for three prescribed sea surface temperature (SST, represented as T_s in this paper) values, 295, 300, and 305K. There is no rotation or land surface, no imposed circulation or dynamic forcing, and the insolation is uniform at every grid-point ($409.6\,\mathrm{Wm}^{-2}$). The RCE simulations (`RCE_large`) were initialized from mean soundings of equilibrated RCE simulations on smaller domains (`RCE_small`) for CRMs. The initial conditions for the `RCE_small` simulations were generated from an approximation of a moist tropical sounding (Wing et al., 2018). There are no aerosol radiative effects. Much of the previous work that discusses the change of overturning circulations with warming (e.g. Held & Soden, 2006; Vecchi & Soden, 2007; Bony & Stevens, 2020) discuss the role of increasing concentrations of CO_2 in reducing the radiative cooling rates. It is important to note that for the RCEMIP experiments studied in this paper the warming is entirely due to increased T_s with no change in the CO_2 concentration, there is no impact from changing CO_2 concentrations on the atmospheric cooling rates in our simulations.

We have analyzed data from 21 of the models that participated in RCEMIP. Descriptions of the models and further details and analysis can be found in Wing et al. (2020) and the supplemental information. Unless noted otherwise, values from GCMs will be displayed with circles and values from CRMs will be displayed with stars. The RCEMIP simulations with prescribed T_s of 295, 300, and 305K are distinguished with increasing marker size. RCEMIP data is publicly available at `http://hdl.handle.net/21.14101/d4beee8e-6996-453e-bbd1-ff53b6874c0e` where it is hosted by the German Climate Computing Center (Deutsches Klimarechenzentrum, DKRZ).

Multiple domain configurations were used by CRMs as part of RCEMIP. Our analysis focuses on the `RCE_large` domain configuration for CRMs and the global domain for GCMs. The CRM `RCE_large` domain is a doubly periodic channel with horizontal dimensions of $\sim 6,000 \times 400\,\mathrm{km}^2$, a model top at ~ 33 km, and a recommendation of using 74 vertical levels. All of the CRMs used a horizontal grid-spacing of 3 km. The GCMs use a horizontal grid-spacing similar to the configuration used by each model for CMIP6 in which ~ 100 km is typical. To consistently compare the CRMs and GCMs, we have coarsened the CRMs to a grid with cells that are $96\,\mathrm{km}^2$ and all GCM data is interpolated to a 1 degree latitude-longitude grid. The experiments using CRMs simulated 100 days, and the last 50 days have been analyzed. The experiments that used the GCMs simulated at least 1000 days, and for this paper we have analyzed the last year of the simulations.

3 Changes of Circulation

Changes in the vertical circulation in the tropics due to warming can be quantified in various ways. Held and Soden (2006) envisioned the exchange of mass M between the BL and the free troposphere to be a useful measure. This constrains M based on the precipitation and the BL mixing ratio. Alternatively, the intensity of the overturning dynamic circulation in the mid-troposphere can be examined using the mean ascending and descending velocities, as in Bony et al. (2013). In the following two subsections we use both of these measures of the tropical circulation to show how the hydrologic cycle and the large-scale circulation change as the surface warms.

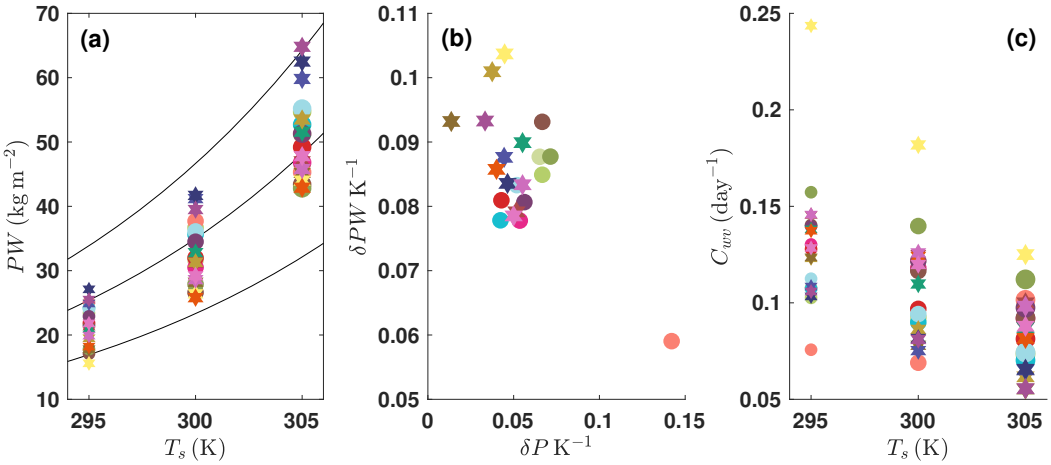

Figure 1: (a) PW as a function of T_s, (b) the differential change of PW and P between the T_s 295K and 305K experiments, (c) and the water vapor cycling rate, C_{wv}, as a function of T_s. GCMs are represented by circles and CRMs by stars.

3.1 Water Vapor cycling and Circulation

The CC relation provides a constraint on the change of the saturation vapor pressure with temperature. Because of this constraint we anticipate an increasing column-integrated water vapor (precipitable water, PW) with increasing surface temperature T_s. All of the RCEMIP models we analyze show an increase of PW with T_s (Fig. 1a). The range of PW across the RCEMIP models for particular T_s values is large ($\sim$ 12, 16, and 22 kg m^{-2} for 295K, 300K, 305K, respectively) and likely indicates different values of surface relative humidity and varying vertical distributions of water vapor. For reference, an analytic function is plotted (black lines) that shows the CC-expected increase of PW as a function of T_s. The three black lines show three particular parameter values that correspond to distinct ratios of the surface relative humidity and the scale height of water vapor (see Appendix A for details, following Stephens, 1990). Although all models show an increase in PW with warming, the range of values at a given T_s and the rate of increase of PW vary widely across models.

Following O'Gorman and Muller (2010), we define the differential change of P as $\delta P = \log(1+\mathrm{r}_\Delta \Delta \mathrm{T_s})/\Delta \mathrm{T_s}$ with $r_\Delta = (P_2 - P_1)/(P_1 \Delta T_s)$ where the subscripts 1 and 2 indicate simulations at T_s of 295 K and 305 K respectively and ΔT_s is 10 K. Differential changes of PW are defined analogously. Previous studies have demonstrated that changes of P in warming experiments, sometimes referred to as the strength of the hydrologic cycle, do not scale with CC but increases at a slower rate (references, e.g., Allen and Ingram, 2002, Flaschner et al?, Boer, 1993?). We find that the change of P with warming is larger than expected based on previous studies (Held & Soden, 2006), but is still smaller than the CC scaling that dominates changes of PW (Fig. 1b). It is worth noting that the CRMs show a smaller range of change in P with a mean value of 4.8%/K. The mean rate of change of PW (8.5%/K) is larger than the value often stated for CC scaling (6.5-7%/K). However, O'Gorman and Muller (2010) showed that the differential change in PW varies strongly in latitude and that tropical values are often between 8-9%/K, consistent with our findings from RCEMIP.

The mean precipitation, P, is not constrained by CC, but rather by the net radiative cooling of the atmosphere. This constraint is not directly tied to T_s but is dependent on the structure of clouds, the precipitation efficiency, and the relative humidity

of the troposphere. According to Betts and Ridgway (1988), the upward mass flux from a convective BL is determined by the ratio of the change in P and the change in the mixing ratio of specific humidity. In the RCEMIP models examined here, the mean rate of change of P ($5.4\%/K$) is substantially less than that of the PW ($8.5\%/K$) but P and PW show considerable spread in both GCMs and CRMs (Fig. 1b). Using PW, rather than the BL mixing ratio to estimate the upward mass flux M we can write $P = M \cdot PW$.

Another way to think about M is as the water vapor cycling rate ($C_{wv} = P/PW$), or the inverse 'residence time' of water vapor. As the surface warms, water vapor stays in the troposphere longer and C_{wv} decreases (Fig. 1c). For example, with a T_s of 295K, the UCLA-CRM model has a residence time ($1/C_{wv}$) of water vapor in the troposphere of about 4 days which increases to 7.7 days in the simulation with a T_s of 305K. Over the same change of T_s the residence time of the CAM5-GCM model increases from 10 to 14.3 days. As the rate of mass exchange (M) between the BL and the free-troposphere decreases, the residence time of water vapor increases. The range of C_{wv} values across the RCEMIP models is large [0.08:0.24] at 295K and [0.06:0.13] at 305K; Fig. 1c. Of the 21 models examined, 20 have $\Delta PW > \Delta P$ (Fig. 1b) and as a result, M and C_{wv} decrease with surface warming in those models (Fig. 1c). The one model for which $\Delta P > \Delta PW$ has an increase of C_{wv} and is thus still consistent with the scaling of Betts and Ridgway (1988) and Held and Soden (2006). The scaling described here relies on the assumption that the distribution of relative humidity will not greatly change as the surface warms. Interestingly, the one model that shows an increase of C_{wv} also shows a large change of the relative humidity with warming in the 305K simulation. Despite the basic physics that is encapsulated by the CC relation and the balance between P and the net radiative cooling, the RCEMIP models still contain enough degrees of freedom to maintain a diverse response to the RCEMIP boundary conditions.

3.2 Intensity of the mid-Tropospheric Overturning Circulation

An alternative to the thermodynamically driven cycling rate of water vapor, C_{wv}, is to calculate the intensity of the large scale overturning circulation as $I = \omega^{\downarrow} - \omega^{\uparrow}$, where $\omega^{\uparrow}$ is the mean upward vertical velocity and $\omega^{\downarrow}$ is the mean downward vertical velocity in the mid-troposphere as approximated on the 500 hPa pressure surface (Bony et al., 2013; Medeiros et al., 2015). In contrast to M and C_{wv}, I directly ties the overturning circulation to the dynamics of the troposphere. Defining the overturning circulation in this way also makes a connection to the subsidence fraction (SF; fraction of domain with subsiding motion at 500 hPa), which is often used as a metric that indicates the degree of convective self-aggregation that is present in an experiment (e.g. Coppin & Bony, 2015; Cronin & Wing, 2017; Wing et al., 2020). Assuming continuity allows one to write an expression for I in terms of SF, $\omega^{\downarrow}$, and $\omega^{\uparrow}$:

$$I = \frac{1}{1-SF}\omega^{\downarrow} = -\frac{1}{SF}\omega^{\uparrow}. \tag{1}$$

We find that for the majority of models the circulation intensity I decreases with warming (Fig. 2a). As discussed by Cronin and Wing (2017), if the subsidence fraction (SF) is relatively constant the implication is that I, $\omega^{\downarrow}$, and $\omega^{\uparrow}$ all scale together as the surface warms. To examine this in the context of the RCEMIP models Fig. 2b shows a scatter plot of I, compared to $\omega^{\downarrow}$ (hollow markers) and $\omega^{\uparrow}$ (filled markers) with lines of constant SF in black (0.5 (thin); 0.8 (2 thick lines)). This helps to illustrate several characteristics of the solutions. The circulation Intensity I scales fairly well with $\omega^{\downarrow}$, $\omega^{\uparrow}$, and SF. This is especially true of for $\omega^{\uparrow}$. The CRMs (stars) tend to have smaller values of I and ω. As T_s increases, the solutions often equilibrate with larger values of SF.

In the subsiding regions of the tropics, often referred to as clear-sky regions, there is a balance between the radiative cooling and adiabatic compression. The subsidence velocity that would balance the radiative cooling in these clear-sky regions is referred

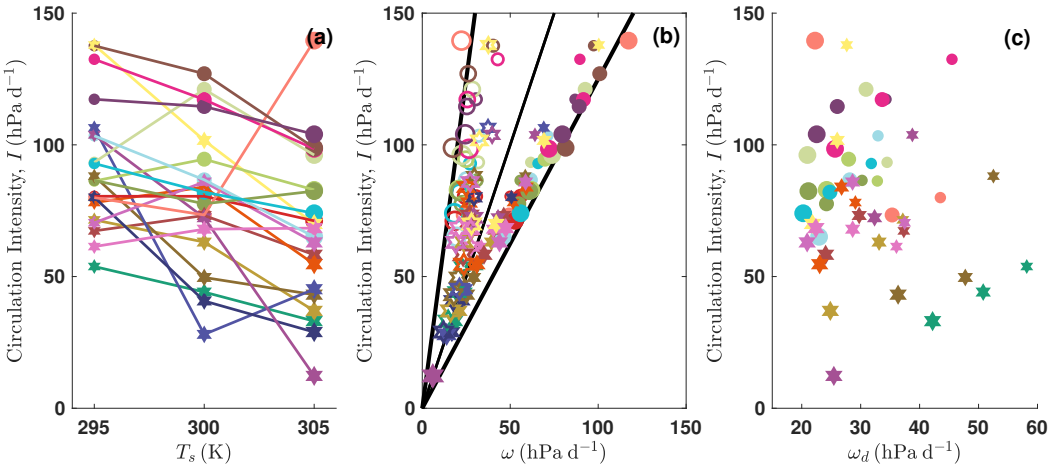

Figure 2: (a) Intensity of the large scale circulation, I, as a function of T_s. (b) Mean upward ($\omega^{\uparrow}$, filled) and downward ($\omega^{\downarrow}$, hollow) components of the vertical velocities. Solid lines show the implied values if the subsidence fraction equal to 0.5 (thin) or 0.8 (two thick lines). (c) Scatter plot of I and the diabatically driven subsidence velocity, ω_d. Circles (stars) indicate GCMs (CRMs) and increasing marker size indicates increases values of T_s. All GCMs have been interpolated to a 1x1 degree grid and the CRMs have been coarsened to cells that are 96km^2. Chunks of 5 days were averaged before computing $I, \omega^{\downarrow}$, or $\omega^{\uparrow}$. Diabatic velocity values have been computed as the mass weighted mean between 200 and 600 hPa.

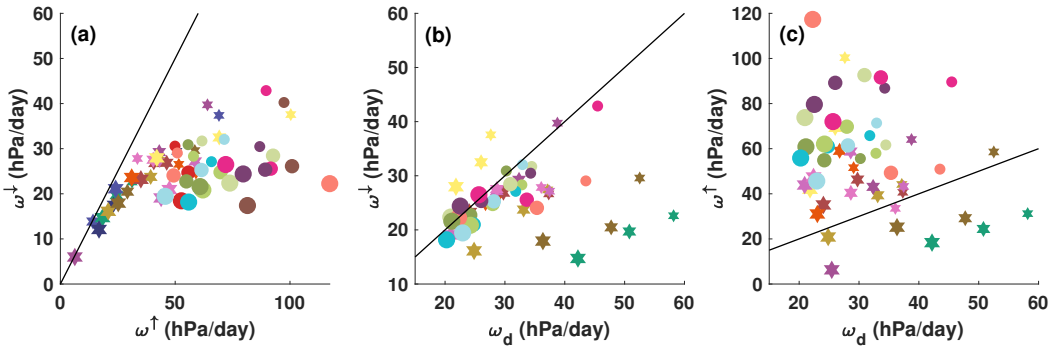

Figure 3: (a) Relationship between the $\omega^{\downarrow}$ and $\omega^{\uparrow}$. (b) Relationship between $\omega^{\downarrow}$ and ω_d. (c) Relationship between the $\omega^{\uparrow}$ and ω_d. For reference black lines show a 1:1 slope. The ω_d has only been computed for models which provided clear sky radiative fluxes. Increasing T_s is indicated by increasing marker size.

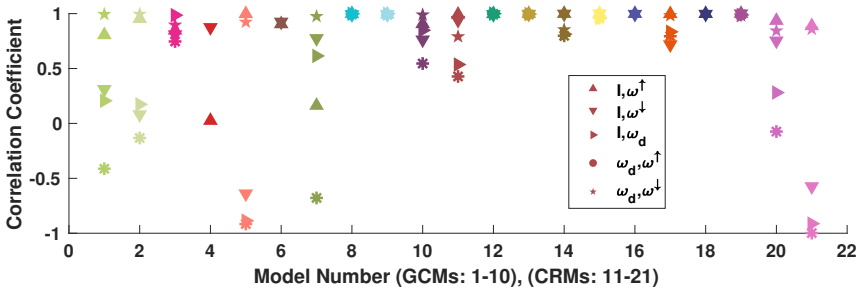

Figure 4: Correlation coefficients have been calculated between I and $\omega^{\uparrow}$, I and $\omega^{\downarrow}$, I and ω_d, ω_d and $\omega^{\uparrow}$, and ω_d and $\omega^{\downarrow}$. Correlation coefficients for each relationship have been calculated over the three T_s simulations for each of the 21 models. Coefficients for particular calculations are indicated by the markers shown in the legend. The ω_d has only been computed for models which provided clear sky radiative fluxes.

to as the radiative, or diabatic, velocity (e.g., Mapes, 2001) and is here given by ω_d. In a steady state tropical atmosphere in which horizontal advection of temperature does not act to modify the temperature, the diabatically driven vertical velocity is approximated as

$$\omega_d \approx Q/\sigma, \tag{2}$$

in which Q is the clear-sky radiative cooling and σ is the static stability. The static stability is given by

$$\sigma = \frac{\partial s/C_p}{\partial p}, \tag{3}$$

with s the dry static energy, p pressure, and C_p the heat capacity at constant pressure. As T_s increases, both I and ω_d decrease for most models (Fig. 2c). However, the relationship between I and ω_d for specific models varies widely. We are interested in the relationship between ω_d and each of I, $\omega^{\uparrow}$, and $\omega^{\downarrow}$. Both observations and theory indicate that the preferred state of the tropical atmosphere maintains broad weakly subsiding regions punctuated by narrow towers of relatively strong ascent (Bjerknes, 1938). The consistency with which $\omega^{\uparrow} \geqslant \omega^{\downarrow}$ in Fig. 3a confirms this tendency among the RCEMIP models. There is a wide range in the values of $\omega^{\uparrow}/\omega^{\downarrow}$ with many of the CRMs having almost the same values of mean upward and downward velocity while the GCMs in some cases have values of $\omega^{\uparrow}$ that are 3-4 larger than $\omega^{\downarrow}$. Scatter plots of $\omega^{\downarrow}$ (Fig. 3b) and $\omega^{\uparrow}$ (Fig. 3c) compared to ω_d reveal a tight relationship between $\omega^{\downarrow}$ and ω_d. This relationship falls near the 1:1 line for most of the GCMs. The scatter among values of $\omega^{\uparrow}$ and ω_d is much broader although some individual models do have a linear relationship (at least for the three simulations examined) between $\omega^{\uparrow}$ and ω_d.

We now illustrate how the variability of I and the change of I with warming compares to the variability of $\omega^{\uparrow}$, $\omega^{\downarrow}$, and ω_d and their changes with warming. Correlation calculations confirm several of the visual impressions from Figs. 1, 2, and 3. Although correlations among sets of three points must be cautiously interpreted, they can be helpful to loosely quantify the relationships. For each model we have calculated the correlations of five relationships: I and $\omega^{\uparrow}$, I and $\omega^{\downarrow}$, I and ω_d, ω_d and $\omega^{\uparrow}$, and ω_d and $\omega^{\downarrow}$. The values are shown in Fig. 4. The largest multi-model correlations (mean of correlations across models) are between ω_d and $\omega^{\downarrow}$ at 0.94 and between I and $\omega^{\uparrow}$ at 0.88. I also has a relatively high correlation with $\omega^{\downarrow}$ of 0.70. The large range of I is very well explained by the range of $\omega^{\uparrow}$ values. Not only does I have a large range of mean values ($44-120\,\mathrm{hPa\,day^{-1}}$), the rate of change with warming of I also varies widely from slightly positive to strongly

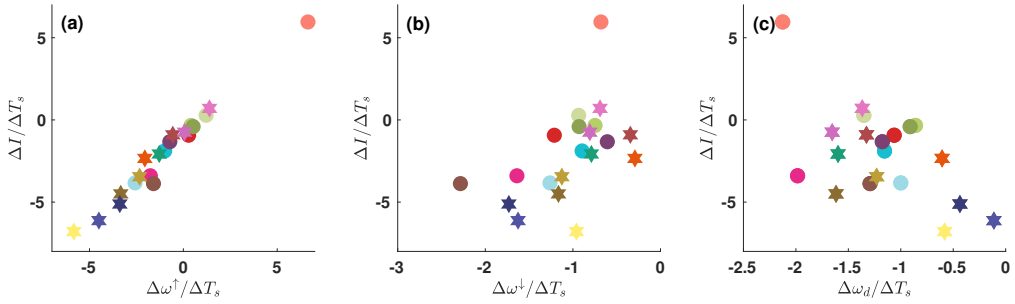

Figure 5: Rates of change with warming ($\mathrm{hPa\,day^{-1}K^{-1}}$). (a) Rate of change of I compared to the rate of change of $\omega^{\uparrow}$. (b) Rate of change of I compared to the rate of change of $\omega^{\downarrow}$. (c) Rate of change of I compared to the rate of change of ω_d. Circles (stars) indicate GCMs (CRMs). Rates have been computed from the best fit polynomial. Correlation coefficients across the ensemble of models are 0.98 (a), 0.67 (b), and -0.47 (c).

negative (Fig. 2). Similar to the range of values of I, the range of values for the slope of I is best explained by the rate of change of $\omega^{\uparrow}$ (Fig. 5a). While Fig. 5 clearly shows a relationship between $\Delta I/\Delta T_s$, $\Delta\omega^{\downarrow}/\Delta T_s$ and $\Delta\omega_d/\Delta T_s$, the strong linear relation between $\Delta I/\Delta T_s$ and $\Delta\omega^{\uparrow}/\Delta T_s$ is striking and confirms the dominant impact that $\omega^{\uparrow}$ and $\Delta\omega^{\uparrow}/\Delta T_s$ have on I and $\Delta I/\Delta T_s$. The large range of changes in I with warming are much better explained by the changes in the mean upward velocity then by the mean subsidence or radiative velocities. This is consistent with recent work that highlights the important role of changes in the ascending regions of the tropics to the strength of the overturning circulation (Jenney et al., 2020; Mackie & Byrne, 2022).

Both of the measures of tropical circulation discussed thus far show a decreasing strength of circulation as T_s increases for the majority of models, but with a large range of magnitudes. We now briefly examine to what extant these measures are related to each other. Figure 6 shows a scatter plot of the fractional rate of change with warming of I compared to the fractional rate of change of C_{wv}. One feature of Fig. 6 that stands out is the fairly tight constraint on the $\Delta C_{wv}/C_{wv}$ near -0.04 for 9 out of 11 CRMs. Several of the GCMs also cluster near this value but overall there is a broader range of possibilities among the GCMs. In contrast to the clustering of the fractional rate of change of C_{wv} around -0.04, the fractional rate of change of I is not constrained in sign and extends over a much wider range. Because the magnitude of both I and $\Delta I/\Delta T_s$ are dependent on the mean value of $\omega^{\uparrow}$, we hypothesize that the spatial structure of the ascending tropical circulations will strongly influence the range of I and $\Delta I/\Delta T_s$ and that the large range seen in Fig. 6 reflects a broad diversity of organized convection and subsidence regions. In contrast, we do not expect C_{wv} to be directly influenced by the structure of the convective regions but rather by thermodynamic and energetic balances. C_{wv} is constrained by both the net atmospheric cooling and the CC relation. Of central importance to the energetic flux that precipitation represents is the net atmospheric cooling, Q, which helps to set the value of ω_d. We hypothesize that the tighter constraint on the value of $\Delta C_{wv}/C_{wv}$ that is apparent in Fig. 6 reflects the smaller range of variability that is present in the subsiding, clear-sky regions of the troposphere as reflected in the small range of variability of $\omega^{\downarrow}$ and ω_d (relative to $\omega^{\uparrow}$) and the high correlation (0.94) between them (Figs. 4, 5).

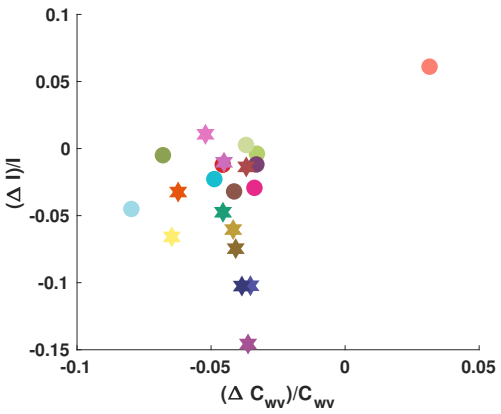

Figure 6: Fractional change of I(hPa day^{-1}K^{-1}) compared to fractional change of the water vapor cycling rate C_{wv} (hPa day^{-1}K^{-1}). The change is computed over the 10K difference between the three RCE simulations.

4 Intermodel Spread of the Overturning Circulation

The previous section showed that both the hydrologic circulation ($C_{wv} \sim P/PW$) and the mean, dynamic overturning circulation (I) decrease with warming for the majority of the RCEMIP models. It was also demonstrated that $\omega^{\uparrow}$ and $\Delta\omega^{\uparrow}/\Delta T_s$ provide the sources of variability in I and $\Delta I/\Delta T_s$, respectively. We would like to better understand the source of the wide range of circulation magnitudes shown in Figs. 1 and 2. In section 4.1 the surface energy budget is discussed along with the implications for variablility in the BL depth, P, and PW. This is important for the range of magnitudes in the hydrologic circulation. Section 4.2 then illustrates some of the sources of variability in the dynamic circulation, I, by looking at the intermodel spread of the radiative cooling, the static stability, and the relative humidity.

4.1 The Surface Energy Flux and Precipitation

The flux of energy from the surface into the atmosphere is a critical component of the tropical atmospheric circulation and its response to warming. The surface energy budget drives the depth of the atmospheric BL which in turn influences the BL humidity and plays a role in the presence of low-level clouds and their response to a warming surface (Rieck et al., 2012). The surface energy fluxes are also important for the temperature and humidity which determine the low level moist static energy. This moist static energy serves as the fuel that triggers deep convective motions which in turn set the tropospheric temperature, generate anvil cloud, and can amplify the deep overturning circulation.

Any hope that the RCE configuration with a prescribed, uniform T_s, uniform insolation, and a consistent surface albedo would lead to similar surface energy fluxes among the RCEMIP models must be abandoned after a cursory look at the data. Both the latent heat flux and the P differ among the models by up to a factor of 2 (Fig. 7), and PW varies by almost as much. The domain mean precipitation, P, is shown in Fig. 7b to vary between about 2.5 mm day^{-1} and 4.5 mm day^{-1}. The range of the Bowen Ratio (ratio of the sensible to latent heat flux) covers more than a factor of two with most of the variations coming from the latent, rather than sensible, heat flux (with the exception of one model). Changes in incoming solar and longwave radiation at the surface will have very little impact on the surface energetics because of the fixed T_s and the low albedo of wa-

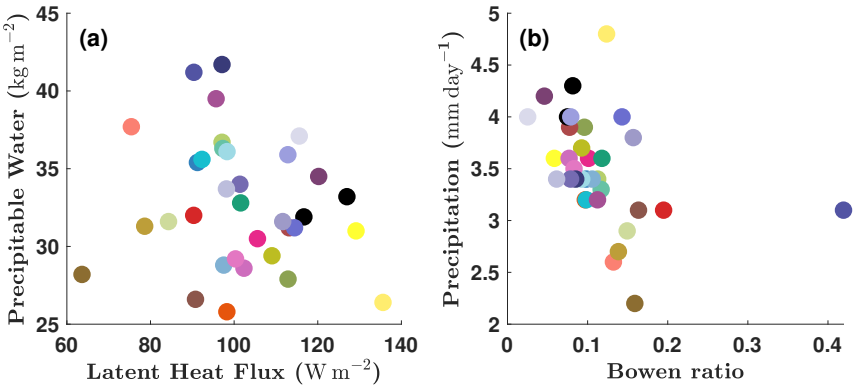

Figure 7: (a) Precipitable Water (PW) as a function of the Latent Heat Flux and (b) Precipitation (P) as a function of the Bowen ratio for the 300K simulations.

ter. As long as the overlying atmosphere remains well coupled to the surface the sensible heat flux does not vary much among models because of the fixed T_s. However, the latent heat flux can and does vary widely across the model ensemble with a range of 64, 72, and 87 W m^{-2} for the 295, 300, and 305K simulations, respectively. The factors that determine how tightly coupled the atmosphere will be to the surface, and consequently what the low-level temperature and humidity will be are critical for determining the sensible and latent heat fluxes. For RCE models using bulk aerodynamic surface flux equations the coupling likely comes down to either the low-level winds or the bulk transfer coefficients. Variations of the low-level temperature and humidity fields, and especially the strong variability of the latent heat flux, will drive a large part of the resulting low-level clouds, the triggering of deep convection, and the variations of P among the models.

Among the RCEMIP models, for a particular T_s, C_{wv} varies by more than a factor of two. This variability is driven by a large range of values in both P and PW. We know that P is tightly constrained by both the latent heat flux and the net atmospheric radiative cooling (e.g. Allen & Ingram, 2002; O'Gorman et al., 2012; Pendergrass & Hartmann, 2014). P is tightly constrained by the latent heat flux and thus the net atmospheric cooling, but the direction of causality between the latent heat flux and the atmospheric cooling in explaining the variability across models is difficult to determine. The large range of values that we see for PW is not constrained by the latent heat flux in any obvious way (Fig. 7a). We hypothesize that the variability of PW among models is driven by differences in the strength of convective mixing and the precipitation efficiency.

4.2 Static Stability and Relative Humidity

Although we have shown that much of the variability of both I and $\Delta I/\Delta T_s$ can be explained by $\omega^{\uparrow}$ and $\Delta\omega^{\uparrow}/\Delta T_s$, the physical processes of the clear sky portions of the domain also play a role in determining the tropical response to warming. Recall that the mean correlation of $\omega^{\downarrow}$ and ω_d among individual models is 0.94. Their similarity in magnitude (at least among GCMs, Fig. 3) has led some previous studies to use ω_d as an approximation for $\omega^{\downarrow}$ (e.g. Mapes, 2001). From equation 2, ω_d is directly proportional to the clear-sky radiative cooling, Q, and inversely proportional to the static stability, σ. Static stability is essentially set by the lapse rate of temperature which thermodynamically connects the convective and clear sky regions of the tropics. Clear sky radiative cooling, Q, is strongly dependent on the tropospheric humidity. Thus ω_d, and by impli-

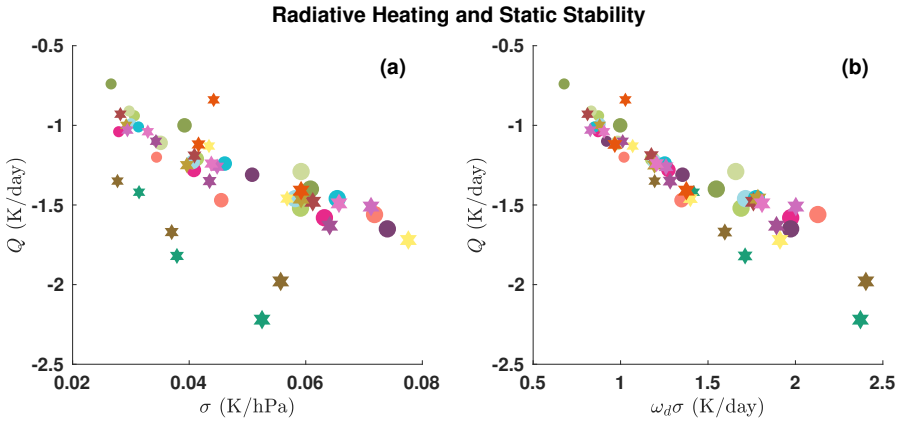

Figure 8: (a) Scatter plot of net radiative heating, Q, and the static stability, σ. (b) The static stability has been scaled by each model's mean ω_d. Increasing marker size indicates experiments with increasing T_s. Vertical mass-weighted averages were taken between 600 and 200 hPa. Includes only the models which saved clear-sky fluxes.

cation ω, while characterizing the clear sky regions of the tropics is closely tied to the deep convection through the dependence of ω_d on the lapse rate of temperature and the RH that is strongly influenced by the deep convection.

To better understand the source of the large spread in ω_d that we find in the RCEMIP simulations, Fig. 8 presents both Q and σ from each simulation. Across the full ensemble of models and all T_s there is a range of $Q \sim 1.5\,\mathrm{K\,day^{-1}}$ and $\sigma \sim 0.05\,\mathrm{K\,hPa^{-1}}$. For each particular T_s there is also substantial spread across the models of both Q ($\sim 1\,\mathrm{K\,day^{-1}}$) and σ ($\sim 0.02\,\mathrm{K\,hPa^{-1}}$) as shown in Fig. 8a. To assist the comparison of the variability between Q (a warming rate) and σ (an inverse length scale) we use the mean of ω_d across the three T_s values for each particular model to scale σ for that particular model in Fig.8b. Somewhat surprisingly, this reveals that both Q and the scaled σ have a range of $\sim 1.5\,\mathrm{K\,day^{-1}}$. We conclude that the large spread in ω_d within the RCEMIP models is due to large variations in both Q and σ and is not dominated by either individually. However, the decrease of ω_d with warming that is apparent in Figs. (2-5) is not due to the changes of Q, it is caused by the robust increase of σ as the surface is warmed (not shown).

Mapes (2001) showed that radiatively driven subsidence, or diabatic velocity, ω_d, drives the drying of the troposphere and leads to a 'C' shaped RH profile. This profile has been noted in observations and discussed theoretically by Romps (2014). The relative humidity profiles in most of the RCEMIP models show the expected mid-tropospheric minimum of RH (Fig. 9 a,d) and the usual 'C' shaped profile. We expect that the range of ω_d values

seen in the RCEMIP models contribute to the enormous range ($\sim 15\% - 85\%$) of mid-tropospheric RH profiles seen in Fig. 9 a,d. Although a large amount of variability in the RH sink term, ω_d, is apparent in Figs. 2,3, and 5, ω_d is not highly correlated with the midtropospheric RH across the model ensemble (not shown). There must be an additional source of the variability in the RH profiles. Both Sherwood et al. (2006) and Romps (2014) argue that in addition to this drying process the steady state mean tropospheric humidity field is the result of a balance that includes both subsidence drying and moistening from convective detrainment. Romps (2014) derived an analytic expression for this balance of moistening and drying:

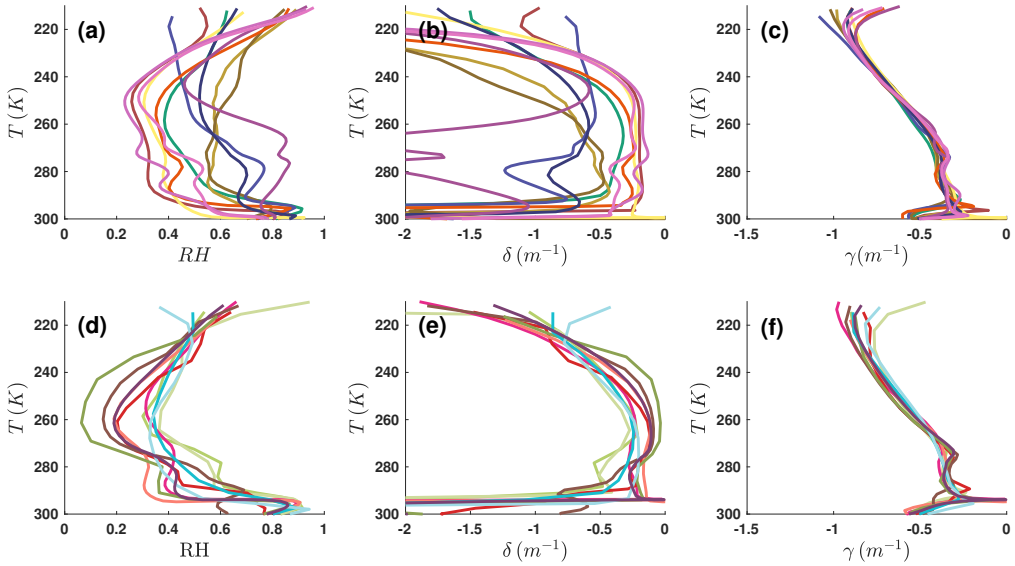

Figure 9: Relative Humidity (left), fractional convective detrainment, δ (middle), and water vapor lapse rate, γ (right). Panels a-c show CRMs and panels d-f show GCMs. All panels show data from the RCE simulation with an T_s of 305K.

$$RH = \frac{\delta}{\delta + \gamma} \tag{4}$$

in which δ is the fractional detrainment rate and γ is the lapse rate of water vapor. The lapse rate of water vapor can be written as a function of only temperature and the lapse rate of temperature (see equation 6 of Romps (2014)). Because the RCE simulations produce the steady state RH and T, we can calculate γ and then the inferred profiles of δ for each model. This is not the actual detrainment as measured from convection in the models, rather, it is the implied detrainment given the equilibrated profiles of RH and T, and assuming that equation 4 is valid. Decomposing RH profiles in this way reveals that most of the range in RH profiles among models is reflected in the inferred δ profiles (Fig. 9b,e) and that the water vapor lapse rate, γ, is quite consistent among the models (Fig. 9c,f). Comparing the RH profiles to the δ profiles offers support to the intuitive idea that models which detrain more moisture from the convective regions will have more moisture in the mean environment. Conversely, the models with the lowest midtropospheric RH values have the smallest amount of inferred detrainment.

The CRMs have a larger (relative to the GCMs) range of RH values in the midtrosphere and a greater diversity of profile shapes, especially so for the 305K simulation shown in Fig. 9. Despite the large range of RH values, the RH profiles remain approximately constant for each model as the T_s increases (generally less than 5% K^{-1}; not shown). The GEOS model is an exception to this and has a large change of the RH between the 300 K and 305 K simulations which could explain why the change of both C_{wv} and I is so different in GEOS relative to the majority of the other models (Figs. 1c and 2a). Given the relatively tight constraints and consistent boundary conditions that the RCEMIP protocol dictated (Wing et al., 2018) it is remarkable how unconstrained the mid-tropospheric RH is among these 21 models. In addition to equation 4 above, Romps (2014) derived a constraint on the precipitation efficiency of $PE \geqslant 1 - RH$. For the models which have drier RH profiles this indicates a substantially higher PE. The wide range of PE and δ that the RH profiles imply among these RCE models could be a reflection of the many varieties of subgrid-scale parameterizations that are employed by

these 21 models. Several 'families' of models can be seen in Fig. 9 to have profiles that group together, perhaps because of overlapping parameterizations. These include the WRF family (WRF-COL-CRM, WRF-CRM: dark plue-purple), the ICON family (ICON-LEM, ICON-NWP: tan-browns), the SP-CAM family (SP-CAM, SPX-CAM: blue-cyan), and the CAM family (CAM5-GCM, CAM6-GCM: light-greens). The UKMO-CRM family (UKMO-CASIM, UKMO-RA1-T, UKMO-RA1-T-nocloud: pink to violet) is a notable exception in which the family members prefer to occupy very different states. A few additioal details are given in Appendix B.

5 Conclusions

Two distinct approaches have been used to quantify the large-scale overturning circulation and measure the change with surface warming. The first measure, the cycling rate of water vapor, C_{wv}, uses the ratio of the mean precipitation (P) and precipitable water (PW) to infer the exchange of mass between the BL and the midtroposphere. The second measure, the intensity, I, of the circulation depends on the midtropospheric vertical velocity. A 21 member ensemble of models from the RCEMIP has been used to calculate the response of the large-scale atmospheric circulation to warming in the context of both global GCMs and large-domain CRMs, all simulating RCE. Robust responses to warming of the models include the following:

- $\Delta C_{wv}/\Delta T_s < 0$ for all but one of the models.
- $\Delta I/\Delta T_s < 0$ for about 90% of the individual models.
- The large range of I and of $\Delta I/\Delta T_s$ are best explained by $\omega^{\uparrow}$ and $\Delta\omega^{\uparrow}/\Delta T_s$, respectively, across the full ensemble of models.
- The fractional change of C_{wv} (about -0.04 ± 0.01) is much more consistent among the models than the fractional change of I.
- $\Delta\omega_d/\Delta T_s < 0$ in all models, driven by increasing static stability, σ.
- $\Delta\omega^{\downarrow}/\Delta T_s < 0$ in all models.
- The static stability, σ, and the mean radiative cooling of the clear sky regions, Q, both increase with warming.

These responses to warming illustrate the relevance of RCE simulations as a tool with which to study physical processes of the Earth's tropical regions and confirm some previously developed understanding of the atmosphere in an idealized setting that permits a wide range of model types. Some understanding of the response of the circulation and atmospheric stability to a warming surface was previously developed through the use of simple models (Betts & Ridgway, 1988), analysis of global climate models (Knutson & Manabe, 1995; Held & Soden, 2006; Vecchi & Soden, 2007; Medeiros et al., 2015), and the analysis of a select number of RCE simulations (Bony et al., 2016; Cronin & Wing, 2017). The present study demonstrates how broadly applicable the basic physics of a decreasing circulation strength with warming is in simulations that use both GCMs and CRMs, adding confidence to our understanding.

The response of the large-scale tropical circulation to warming that we have illustrated with these results from RCEMIP demonstrates the interlocking relationships among many of the key variables. Increasing T_s leads to an increased static stability, σ, and a correspondingly smaller diabatic velocity, ω_d. Warmer surface temperatures also lead to larger fluxes of latent heat from the surface and more domain mean precipitation which is eventually reflected in the net atmospheric cooling to space. The radiative cooling to space is strongly influenced by the distribution of clouds and the increased precipitable water that is dictated by the CC relation. The utility of RCE simulations is confirmed by the fact that these same interlocking relationships act in the observed tropical atmosphere of Earth and in many comprehensive GCMs (Knutson & Manabe, 1995; Bony et al., 2016). One of the most interesting results of this multi-model comparison is the ex-

tent to which the equilibrated climate can still vary among models within the framework of this response to warming. The latent heat flux for example, is expected to increase with warming, but for individual models that increase turns out to range from about $10\,\mathrm{W\,m^{-2}K^{-1}}$ to less than $1\,\mathrm{W\,m^{-2}K^{-1}}$. Both the GCMs and the CRMs display similarly large ranges of variability among basic variables such as σ and PW. This confirms what has been known for years, that increased resolution alone will not eliminate the uncertainty that is present in our models. Although GCMs are sensitive to resolution (Reed & Medeiros, 2016; Herrington & Reed, 2020), a better understanding of the parameterized moist processes is essential. Simulations of RCE can facilitate tests of our process-level understanding of convective parameterizations and microphysics. Analysis of the RCEMIP simulations in the CAM5 and CAM6 GCMs has shown that major differences in the low-level clouds, which are in part due to differences in parameterized convection and BL processes, are also reflected in the tropical clouds of the parent models, CESM1 and CESM2 (Reed et al., 2021). Reed et al. (2021) also documented an official public release of the RCEMIP setup in CAM (QPRCEMIP) that should be used by the wider community for additional RCE studies.

Some of the previous studies that illustrated the weakening of the tropical circulation of coupled Earth-like global climate models in response to a warming climate (Knutson & Manabe, 1995; Vecchi & Soden, 2007) found that the Walker circulation was the component of the tropical overturning circulation that decreased in magnitude. The fact that RCE models of the tropical circulation with uniform T_s reproduce this change of circulation with warming implies that the change of circulation is not driven by changes in the pattern of T_s that is characteristic of the Walker Circulation, but rather due to basic physical processes of the atmosphere as argued by both Knutson and Manabe (1995) and Held and Soden (2006). Nevertheless, the wide range of variability we find in both the circulation and the change of circulation with warming could be partly due to an underconstrained system. Several previous studies (Jeevanjee et al., 2017; Cronin & Wing, 2017; Silvers & Robinson, 2021) have hypothesized that imposing a mock-Walker Circulation on models of RCE could help to increase the applicability of the results, relative to strict RCE. A mock-Walker circulation is probably the simplest way to incorporate forced large-scale circulations into the balance between radiation and convection and is one step closer to the observed tropical atmosphere. This would provide a potentially fruitful comparison between GCMs and CRMs. But more importantly, utilizing the mock-Walker circulation in an RCE-like setting would highlight interactions between the tropical circulations, radiation, and cloud systems in a context that should lead to a better understanding of the role that clouds play in Earth's climate.

Appendix A Changes of Water Vapor with Warming according to the Clausius-Clapyron Relation

The Clausius-Clapeyron relation can be written as

$$\frac{de^*}{dT} = \frac{Le^*}{RT^2} \tag{A1}$$

where R is the gas constant for water, e^* is the saturation vapor pressure, L represents the latent heat of condensation and T is the temperature. Following Stephens (1990), this equation can be approximated as

$$e_0^* = 17.044 e^{a(T_s - 288)} \tag{A2}$$

in which T_s is the SST and $a \approx 0.064\,k^{-1}$. Using (A2) Stephens then derives an approximate relationship between precipitable water ($PW, \mathrm{kg\,m^{-2}}$) and T_s as

$$PW = 108.2 \left(\frac{r}{1+\lambda} \right) e^{a(T_s - 288)}. \tag{A3}$$

In (A3) r is the surface value of relative humidity and H/λ is the scale height of water vapor if H is the atmospheric scale height. Typical values of H and λ are 7 km and 3.5, respectively. The three black lines in the left panel of Fig. 1 show (A3) plotted with three values of the coefficient $r/(1+\lambda)$: 0.1, 0.15, and 0.2.

Appendix B Technical Notes on specific RCEMIP models

Many of the characteristics both of the large-scale circulation, and of tropical convection are dependent on the BL and the subcloud layer energy. The vertical and horizontal resolution of GCMs near the surface is therefore of interest as a possible difference of note between the models. The overview paper for initial RCEMIP results, (Wing et al., 2020) specified that the participating GCMs would employ the grids which they used for CMIP6. The result of this is that the GCMs in RCEMIP represent a very wide range of vertical grids, with one model having only 26 vertical levels and another having 91. The horizontal resolutions are difficult to compare directly because of the different grids, but the grid spacing ranges from approximately 100 km to around 160 km. Of the 11 GCMs which participiated in RCEMIP, 6 of them place the model level which is closest to the surface at 64m (CAM5, CAM6, SP-CAM, SPX-CAM, SAM-UNICON, and GEOS). The IPSL, ECHAM, and ICON models place their lowest level at 49, 33, and 20m, respectively. The CNRM and UKMO GCMs both have the lowest model level at just 10m above the surface. Initial findings (scatter plots not shown here) indicate that the height of the lowest atmospheric model level does not play a clear role in driving characteristics of the RCE experiments. It is well known that grid spacing in GCMs influences fundamental characteristics of the climate such as cloud distributions and the relative humidity (e.g. Reed & Medeiros, 2016; Herrington & Reed, 2020). An intercomparison of GCMs running RCE using the same grid would be useful.

Among the CRMs that completed simulations on the large domain there are a few 'families' of models that share some components. The list below details this in extreme brevity, further specifications of RCEMIP models can be found in the supporting information of Wing et al. (2020).

- **UKMO:** The configurations of the UKMO-CASIM, UKMO-RA1-T and UKMO-RA1-T-nocloud are very similar to each other. UKMO-CASIM can be thought of as the base model. UKMO-RA1-T has different microphysics and uses a sub-grid cloud scheme. The UKMO-RA1-T-nocloud simply disable this sub-grid cloud scheme.
- **WRF:** WRF-COL-CRM and WRF-CRM are very different models. The radiation schemes, the microphysics, and the turbulence schemes all differ. However, they both uses double moment microphysics (but not the same scheme). They have the same BL scheme, but different sub-grid turbulence. The multiple ensembles of the WRF-GCM are based off of the WRF-COL-CRM model.
- **ICON:** The two ICON CRMs (ICON-LEM and ICON-NWP) use the same dynamical core, grid, parameterization of longwave and shortwave radiation (RRTMG), and two-moment mixed phase bulk microphysics scheme (Seifert & Beheng, 2006). The parameterizations for BL turbulence, subgrid-scale turbulence, and cloud cover differ.

Acknowledgments

Silvers and Reed acknowledge support from NSF award number 1830729, Wing acknowledges support from NSF award number 1830724. We are grateful to the German Climate Computing Center (DKRZ) where the RCEMIP data is hosted. RCEMIP data is publicly available at `http://hdl.handle.net/21.14101/d4beee8e-6996-453e-bbd1-ff53b6874c0e`. We thank all RCEMIP contributors for providing the RCEMIP simulations. We thank

Michael Byrne and Anna Mackie for helpful conversations during the development of this research. High-performance computing support was provided by NCAR's Computational and Information Systems Laboratory through the computer Cheyenne (doi:10.5065/D6RX99HX). NCAR is sponsored by the National Science Foundation.

References

Allen, M. R., & Ingram, W. J. (2002). Constraints on future changes in climate and the hydrologic cycle. *Nature*, *419*, 228-232. doi: 10.1038/nature01092

Betts, A. K., & Ridgway, W. (1988). Coupling of the radiative, convective, and surface fluxes over the equatorial pacific. *Journal of Atmospheric Sciences*, *45*(3), 522 - 536. doi: 10.1175/1520-0469(1988)045⟨0522:COTRCA⟩2.0.CO;2

Bjerknes, J. (1938). Saturated-adiabatic ascent of air through dry-adiabatically descending environment. *Quart. J. Roy. Meteor. Soc.*, *64*, 325–330.

Bony, S., Bellon, G., Klocke, D., Sherwood, S., Fermepin, S., & Denvil, S. (2013). Robust direct effect of carbon dioxide on tropical circulation and regional precipitation. *Nature Geoscience*, *6*(6), 447–451. doi: 10.1038/ngeo1799

Bony, S., Dufresne, J. L., Treut, H. L., Morcrette, J.-J., & Senior, C. (2004). On dynamic and thermodynamic components of cloud changes. *Clim. Dynam.*, *22*. doi: 10.1007/s00382-003-0369-6

Bony, S., & Stevens, B. (2020). Clouds and warming. In A. P. Siebesma, S. Bony, C. Jakob, & B. Stevens (Eds.), *Clouds and climate* (p. 356-388). Cambridge University Press.

Bony, S., Stevens, B., Coppin, D., Becker, T., Reed, K. A., Voigt, A., & Medeiros, B. (2016). Thermodynamic control of anvil cloud amount. *Proceedings of the National Academy of Sciences*, *113*(32), 8927–8932. doi: 10.1073/pnas.1601472113

Bretherton, C. S., & Sobel, A. H. (2002). A simple model of a convectively coupled walker circulation using the weak temperature gradient approximation. *Journal of Climate*, *15*(20), 2907-2920. doi: 10.1175/1520-0442(2002)015⟨2907:ASMOAC⟩2.0.CO;2

Coppin, D., & Bony, S. (2015). Physical mechanisms controlling the initiation of convective self-aggregation in a general circulation model. *J. Adv. Model. Earth Syst.*, *7*. doi: 10.1002/2015MS000571

Cronin, T. W., & Wing, A. A. (2017). Clouds, circulation, and climate sensitivity in a radiative-convective equilibrium channel model. *Journal of Advances in Modeling Earth Systems*, *9*(8), 2883-2905. doi: 10.1002/2017MS001111

Grabowski, W. W., Yano, J.-I., & Moncrieff, M. W. (2000). Cloud resolving modeling of tropical circulations driven by large-scale sst gradients. *Journal of the Atmospheric Sciences*, *57*(13), 2022-2040. doi: 10.1175/1520-0469(2000)057⟨2022:CRMOTC⟩2.0.CO;2

Held, I. M., & Soden, B. J. (2006). Robust responses of the hydrological cycle to global warming. *Journal of Climate*, *19*(21), 5686 - 5699. doi: 10.1175/JCLI3990.1

Herrington, A. R., & Reed, K. A. (2020). On resolution sensitivity in the Community Atmospheric Model. *Quarterly Journal of the Royal Meteorological Society*, *146*, 3789-3807. doi: 10.1002/qj.3873

Jeevanjee, N., Hassanzadeh, P., Hill, S., & Sheshadri, A. (2017). A perspective on climate model hierarchies. *Journal of Advances in Modeling Earth Systems*, *9*(4), 1760-1771. doi: 10.1002/2017MS001038

Jenney, A., Randall, D., & Branson, M. (2020). Understanding the response of tropical ascent to warming using an energy balance framework. *Journal of Advances in Modeling Earth Systems*, *12*. doi: 10.1029/2020MS002056

Knutson, T. R., & Manabe, S. (1995). Time-mean response over the tropical pacific to increased c02 in a coupled ocean-atmosphere model. *Journal of Climate*,

8(9), 2181 - 2199. doi: 10.1175/1520-0442(1995)008⟨2181:TMROTT⟩2.0.CO;2

Lutsko, N. J., & Cronin, T. W. (2018). Increase in precipitation efficiency with surface warming in radiative-convective equilibrium. *JAMES*, *10*, 2992-3010. doi: 10.1029/2018MS001482

Mackie, A., & Byrne, M. P. (2022). *Effects of circulation on tropical cloud feedbacks in high-resolution simulations.* (in review)

Mapes, B. (2001). Water's two height scales: The moist adiabat and the radiative troposphere. *Quart. J. Roy. Meteor. Soc.*, *127*, 2353–2366.

Medeiros, B., Stevens, B., & Bony, S. (2015). Using aquaplanets to understand the robust responses of comprehensive climate models to forcing. *Climate Dynamics*, *44*(7-8), 1957–1977.

O'Gorman, P. A., Allan, R. P., Byrne, M., & Previdi, M. (2012). Energetic constraints on precipitation under climate change. *Surveys in Geophysics*, *33*, 585–608. doi: 10.1007/s10712-011-9159-6

O'Gorman, P. A., & Muller, C. J. (2010). How closely do changes in surface and column water vapor follow Clausius-Clapeyron scaling in climate simulations? *Environmental Research Letters*, *5*, 025207. doi: 10.1088/1748-9326/5/2/025207

Pendergrass, A. G., & Hartmann, D. L. (2014). The atmospheric energy constraint on global-mean precipitation change. *Journal of Climate*, *27*(2), 757 - 768. doi: 10.1175/JCLI-D-13-00163.1

Raymond, D. J. (1994). Convective processes and tropical atmospheric circulations. *Quarterly Journal of the Royal Meteorological Society*, *120*(520), 1431-1455. doi: 10.1002/qj.49712052002

Reed, K. A., & Medeiros, B. (2016). A reduced complexity framework to bridge the gap between AGCMs and cloud-resolving models. *Geophys. Res. Lett.*, *43*, 860-866. doi: 10.1002/2015GL066713

Reed, K. A., Silvers, L. G., Wing, A. A., Hu, I.-K., & Medeiros, B. (2021). Using radiative convective equilibrium to explore clouds and climate in the Community Atmosphere Model. *J. Adv. Model. Earth Syst.*, *13*. doi: 10.1029/2021MS002539

Romps, D. M. (2014). An analytical model for tropical relative humidity. *Journal of Climate*, *27*(19), 7432–7449.

Seifert, A., & Beheng, K. (2006). A two-moment cloud microphysics parameterization for mixed-phase clouds. part 1: Model description. , *92*, 45-66. doi: 10.1007/s00703-005-0112-4

Shepherd, T. G. (2014). Atmospheric circulation as a source of uncertainty in climate change projections. *Nature Geoscience*, *7*(10), 703—708. Retrieved from `https://doi.org/10.1038/ngeo2253`

Sherwood, S. C., Kursinski, E. R., & Read, W. G. (2006). A distribution law for free-tropospheric relative humidity. *Journal of Climate*, *19*(24), 6267 - 6277. doi: 10.1175/JCLI3978.1

Sherwood, S. C., Webb, M. J., Annan, J. D., Armour, K. C., Forster, P. M., Hargreaves, J. C., ... Zelinka, M. D. (2020). An assessment of Earth's climate sensitivity using multiple lines of evidence. *Rev. Geophys.*, *58*. doi: 10.1029/2019RG000678

Silvers, L. G., & Robinson, T. (2021). Clouds and radiation in a mock-walker circulation. *J. Adv. Model. Earth Syst.*, *13*. doi: 10.1029/2020MS002196

Tompkins, A. M. (2001). On the relationship between tropical convection and sea surface temperature. *Journal of Climate*, *14*(5), 633-637. doi: 10.1175/1520-0442(2001)014⟨0633:OTRBTC⟩2.0.CO;2

Vecchi, G. A., & Soden, B. J. (2007). Global warming and the weakening of the tropical circulation. *Journal of Climate*, *20*(17), 4316-4340. doi: 10.1175/JCLI4258.1

Voigt, A., & Shaw, T. A. (2015). Circulation response to warming shaped by radia-

tive changes of clouds and water vapour. *Nat. Geosci.*, *8*(2), 102-106. doi: 10.1038/ngeo2345

Wing, A. A., Reed, K. A., Satoh, M., Stevens, B., Bony, S., & Ohno, T. (2018). Radiative–convective equilibrium model intercomparison project. *Geoscientific Model Development*, *11*(2), 793–813. Retrieved from `https://www.geosci-model-dev.net/11/793/2018/` doi: 10.5194/gmd-11-793-2018

Wing, A. A., Stauffer, C. L., Becker, T., Reed, K. A., Ahn, M.-S., Arnold, N. P., ... Zhao, M. (2020). Clouds and convective self-aggregation in a multimodel ensemble of radiative-convective equilibrium simulations. *Journal of Advances in Modeling Earth Systems*, *n/a*(n/a), e2020MS002138. doi: 10.1029/2020MS002138